coatings

MDPI

Article

Use of Organic Acids as Additives for Plasma Electrolytic Oxidation (PEO) of Titanium

Federica Ceriani *, Luca Casanova and Marco Ormellese

Department of Chemistry, Materials and Chemical Engineering "G. Natta", Politecnico di Milano, Via Mancinelli 7, 20131 Milano, Italy; luca.casanova@polimi.it (L.C.); marco.ormellese@polimi.it (M.O.)
* Correspondence: federica.ceriani@polimi.it

Abstract: The present study investigates the influence of organic acids, added to the electrolytic solution, on the structure, morphology, and corrosion behaviour of plasma electrolytic oxidation (PEO) coatings produced on titanium grade 2. Particular attention is paid to the role of functional groups in the modification of the oxide's properties. For this reason, all three selected acids, namely glutaric, glutamic, and tartaric acid, display two carboxylic groups, thus they interact with the substrate material mainly through $–COO^-$ adsorption. However, glutamic acid also has an amine group, while tartaric acid has two hydroxyl groups. The presence of such additional functional groups is found to impact the formation of the PEO coatings. According to scanning electron microscopy (SEM) analyses, the number of defects and their dimension increase with an increasing number of active groups present in the organic molecules. Then, when glutaric acid with only two carboxyl groups, is employed as an additive, smaller pores are produced. The dimension of defects increases when glutamic and tartaric acid are used. X-ray diffraction (XRD) testing demonstrates that rutile and anatase are present in all the coatings and that when using tartaric acid, a relatively high level of amorphism is reached. The electrochemical and corrosion behaviours are evaluated by potentiodynamic polarization (PDP) and electrochemical impedance spectroscopy (EIS) performed in a heated sulphuric acid solution. It is found that all types of coatings provide protection against corrosion, with oxides produced using glutamic acid showing the lowest corrosion current density (0.58 $mA \cdot m^{-2}$) and low corrosion rate (1.02 $\mu m \cdot y^{-1}$).

Keywords: PEO; titanium; organic acid; carboxyl group; corrosion; coating; EIS

Citation: Ceriani, F.; Casanova, L.; Ormellese, M. Use of Organic Acids as Additives for Plasma Electrolytic Oxidation (PEO) of Titanium. *Coatings* **2024**, *14*, 703. https://doi.org/10.3390/coatings14060703

Academic Editor: Yingliang Cheng

Received: 8 May 2024
Revised: 29 May 2024
Accepted: 30 May 2024
Published: 3 June 2024

1. Introduction

Titanium and titanium alloys are commonly used in several applicational fields, such as automotive, chemical, aerospace, marine, biomedicine, and food industries. This is thanks to their great combination of properties like mechanical stability, high strength-to-weight ratio, low density, high biocompatibility, rather high melting point, and great corrosion resistance [1].

The enhanced corrosion resistance under a wide range of conditions is due to the formation of a protective layer made of titanium dioxide (TiO_2) on the metal surface. Such film is spontaneously generated when Ti comes in contact with the atmosphere and its maximum thickness generally does not exceed about 10 nm. Despite the good chemical stability and adhesion to the substrate of the native oxide layer, there are some particularly aggressive conditions, like environments containing fluorides, bromides, or strongly acidic conditions, under which the thin oxide layer can undergo rapid dissolution [2].

Consequently, to improve the corrosion protection of titanium, surface treatments could be performed in order to boost the formation of a thicker TiO_x layer on its surface. Different types of processes could be employed, both physical and chemical. Some examples are physical (PVD) and chemical (CVD) vacuum deposition, sol-gel treatments and thermal or plasma spray. However, all these techniques present some limitations

mainly associated with the low coating rate, the poor adhesion between the coating and the substrate, the high energy consumption and the complexity of the technological setup [3,4]. An alternative and promising method for surface treatment of titanium, that overcomes several of the above-mentioned disadvantages, is plasma electrolytic oxidation (PEO). This electrochemical technique allows an increase in the thickness of the oxide from tens of nm up to 100–200 μm. PEO consists of anodic oxidation of metals or alloys in aqueous solutions performed at high voltages under the condition of plasma discharge. The discharge promotes local high pressure and temperature causing complex plasma-chemical reactions to occur contributing to the stabilization of ceramic-like structures [5].

The main characteristics of these PEO coatings are high adhesion to the substrate, good thermal stability, mechanical strength, and hardness. Unfortunately, their structure is affected by the presence of micro defects and pores connected by channels that significantly reduce the corrosion resistance, since aggressive species can easily penetrate and reach the metallic substrate where corrosion may occur. The formation of such morphological defects is directly related to the PEO coating formation mechanism, making the electrode surface continuously subjected to impervious cycles of thermal loads [6].

Nonetheless, upon the control of specific technological parameters, like the composition of the bath, it is possible to smooth out such defective regions. Depending on the nature of the electrolytic solution, different conditions of dynamical equilibrium between oxide film formation and dissolution are established, influencing the oxide growth behaviour. Moreover, selecting proper molecules with different adsorption capabilities (owing to proper functional groups) onto the titanium substrate. it is possible to smooth the detrimental action of the plasma [7].

Among all the possible types of electrolytes that can be used to modify the PEO regime, attention will be focused on electrolytic solutions containing organic compounds. In particular, to work regardless of the effect of the cationic species, organic acid will be considered in the present work. Generally, when organic substances are added to a base alkaline solution, they tend to interact with the surface of the metallic substrate, and form oxides through their functional groups (–OH, –NH, –COOH, –CO–, etc.). Thus, the organic substances will be incorporated in the final coating generating a hybrid organic-inorganic (HOI) material that could be defined as a micro-composite able to combine the unique properties of both types of materials [8].

In particular, the addition of three organic acids, namely glutaric, glutamic, and tartaric acid, to the electrolytic solution will be analysed. Amino acids (glutamic acid) and carboxylic acids are commonly used as corrosion inhibitors, especially for copper, steel, and aluminum. The interaction between the metal and the organic molecules generally occurs through the carboxyl group, –COOH, via electron donation ($–COO^-$) and leads to the formation of a protective film of molecules [9,10].

Glutaric acid ($C_5H_8O_4$) is an aliphatic carboxylic acid that interacts with the metallic surface by adsorption through the –COOH group on the cathodic sites of the corroding metal leading the alkyl chain of the molecule projected into the solution and causing the formation of a barrier layer with an electron repelling character [10].

Glutamic acid ($C_5H_9NO_4$) is characterized by the presence of an amine group and two carboxyl groups and thanks to its structure it has the ability to coordinate with metals efficiently covering their surface and forming a stable chelate system. The adsorption of glutamic acid on the titanium surface is studied under the conditions of polarization at low anodic potentials (0.5–1.0 V/SSC) in alkaline solutions. For pH > 7, the carboxylic groups of glutamic acid are deprotonated, thus they interact electrostatically and coordinate with the oxide layer on the titanium surface when the substrate is experiencing anodic polarization (positively charged surface). Depending on the polarization potential one or both the carboxyl groups of the acid can be involved in coordination with the metal, if the voltage is lower than 750 mV only the distal group takes part in the interaction, while at higher potentials, the proximal group also is involved [11,12].

Tartaric acid ($C_4H_6O_6$) is characterized by the presence of two carboxyl groups and two hydroxyl groups [12].

The effect of tartaric acid addition in the PEO electrolyte is analysed in both acidic and alkaline electrolytes. It is found that adding tartaric acid to sulphuric acid electrolytes reduces the intensity of oxygen evolution inside the anodic film and the dissolution rate of the oxide layer. As a result, the growth rate of the oxide film on titanium alloys increases [13]. Regarding the addition of tartaric acid to an alkaline electrolyte, it is observed that it leads to a decrease of pore dimensions [14].

The aim of the present paper is to study the influence of the addition of organic anions to the PEO solution in order to promote the formation of thick and compact ceramic layers. In particular, two carboxylic acids and one amino acid will be studied. All three compounds contain carboxyl functional groups, responsible for strong interaction with the substrate. It will be shown that upon the addition of other functional groups such as hydroxides or amine groups, it is possible to modulate the charge transfer and so the level of plasma developing at the interfacial region of the electrode, dictating important features like thickness, morphology, elemental composition, and corrosion resistance.

2. Materials and Methods

The PEO treatment is carried out over 10 × 10 × 1.6 mm^3 Ti grade 2 (UNS R50400) squared samples. The electrolytic bath consists of an alkaline solution of 1 M NaOH and 0.03 M Na_2SiO_3, containing the addition of 0.04 M of different organic acids (glutaric, glutamic, and tartaric), data are summarized in Table 1. The solution is stirred using a magnetic anchor rotating at 600 rpm, for preventing mass transfer limitations and maintaining homogenous temperature within the electrolyte. The process is performed in 500 mL of solution in a Pyrex beaker using as counter electrode, a cylindrical net made of activated titanium placed around the titanium coupon. PEO is performed using an AC/DC power source (California Instruments Asterion 751). The applied signal consists of a duty cycle 60A%–40C%–7CP% ("A" and "C" indicating anodic and cathodic polarization, respectively, and CP meaning the % of cathodic polarization applied with respect to the anodic one) repeated at 1000 Hz. The pulsed signal is provided under a potentiostatic regime considering a final voltage of 90 V achieved through a 320 s time ramp.

Table 1. Electrolytic solutions composition.

Sample	Base Solution	Type of Organic Additive	Concentration of Organic Additive
PEO-GR PEO-GM PEO-TA	NaOH 1 M + 0.03 M Na_2SiO_3	Glutaric acid Glutamic acid Tartaric acid	0.04 M

During PEO treatments the voltage and current responsesare recorded using a Tektronix TBS-1072B-EDU oscilloscope.

In situ optical emission spectroscopy (OES) is executed using an Ocean Optics S2000 spectrometer equipped with an optical fibre P400-1-UV-VIS, allowing an overall spectral resolution of ~0.3 nm in a window between 300 ÷ 1100 nm.

The morphology of PEO oxide is investigated through a Carl Zeiss EVO 50VP SEM (ZEISS, Oberkochen, Germany). For energy dispersive spectroscopy (EDS) a Bruker X-ray spectrometer equipped to the SEM instrumentation is used. X-ray diffraction (XRD) analyses, performed using a Philips PW3020 goniometer with Cu Kα1 radiation (1.54058 Å), make it possible to determine the crystal structure of the coating. Glow discharge optical emission spectroscopy (GD-OES) is performed to determine the oxide elemental composition by using a SpectrumA ANALYTIK GDA 750 HR analyser (Spectruma, Hof, Germany).

Electrochemical tests are performed using a Metrohm Autolab PGSTAT, employing a standard three-electrode cell with an Amel Pt counter electrode and a KCl saturated silver/silver chloride (SSC) reference electrode. The corrosion behaviour of the PEO

samples is investigated through potentiodynamic polarization (PDP) and electrochemical impedance spectroscopy (EIS) analyses. PDP measurements are performed at a scan rate of 10 mV·min^{-1} by polarizing the sample at ±250 mV with respect to E_{corr}. EIS is carried out in a 10% *v*/*v* sulphuric acid solution heated to 60 °C, working within a frequency window of $10^5 \div 10^{-2}$ Hz, applying a sinusoidal signal having an amplitude of 10 mV_{rms} and collecting 10 points per decade of frequency.

3. Results

3.1. Voltage and Current Response

The voltage (*V*)-time plots of PEO samples are displayed in Figure 1. It is \ noted that voltage peaks overcoming 90 V are produced, especially in the last stages of the process (from 280 s). This is particularly true for PEO-GM (Figure 1a) and PEO-GR (Figure 1b) which are characterized by the presence of surges reaching ~147 V and ~142 V, respectively. Concerning PEO-TA (Figure 1c) a smoother *V* ramp is observed.

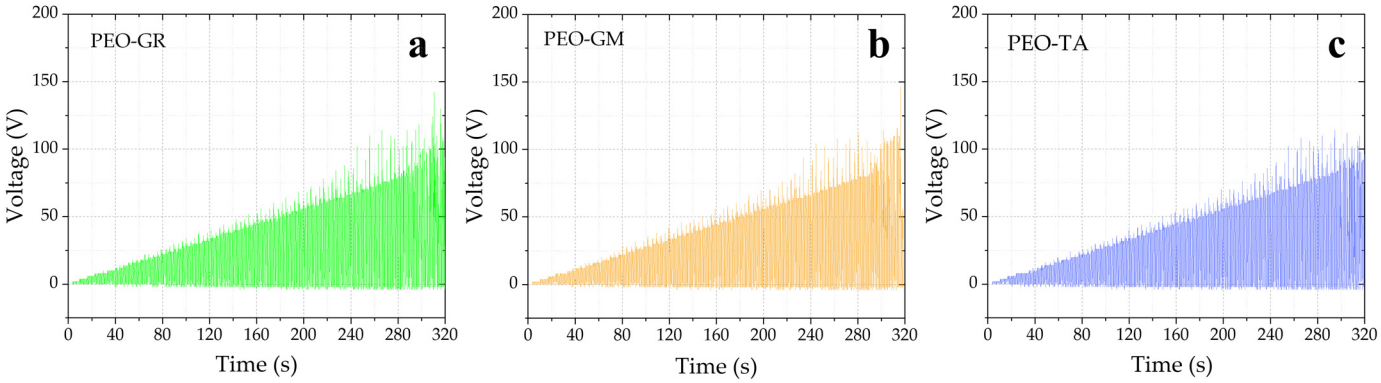

Figure 1. Voltage–time trend of PEO-treated samples in (**a**) glutaric, (**b**) glutamic, and (**c**) tartaric acids.

The anodic portion of the current duty cycle, collected after 300 s of treatment, is plotted and fitted by an exponential decay function, the black curve of Figure 2a. The current (*I*)-time plot (Figure 2) shows a profile common to all the samples. After an initial capacitive peak, related mainly to the charging of the double layer, *I* decays to a plateau with values around 1.25 A·cm^{-2} for PEO-GR and about 2.5 A·cm^{-2} for the other two samples. Only the anodic portion is plotted as no noticeable differences are encountered during the cathodic half-cycle.

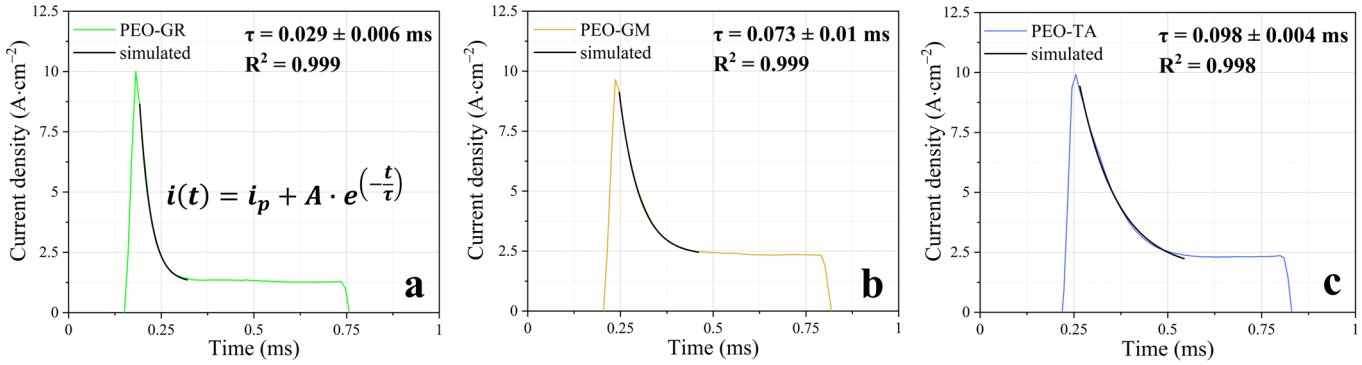

Figure 2. Current–time trend of PEO-treated samples in (**a**) glutaric, (**b**) glutamic, and (**c**) tartaric acids.

The decaying current trend is fitted according to a simple exponential decay function in order to extrapolate the time constant governing the double layer relaxation. This contribution is useful to get insight into the influence of the different anions adsorbed at the interfacial region during the anodic polarization which strongly depends on the presence of certain functional groups, like carboxylic, and on the mobility of the anions subjected to the

high field process. Indeed, the kinetics are directly related to the mobility by which anions move further away from the adsorption sites located in the electrical double layer and subjected to repeated anodic and cathodic cycles occurring every 1 ms (1000 Hz). Thus, the retention and consequent adsorption of organic anionic species, over the electrode surface, can contribute to control the development of plasma [15,16].

3.2. Characterization of the PEO Process

OES spectra, collected after 300 s of treatment, (Figure 3) reveal that elements of both the electrolyte (such as Si, Na, C) and the substrate (Ti) take part in the discharge process and that the most intense lines belong to Ti, O, C and Si species. In particular, intense signals associated with Si II and C I are recorded.

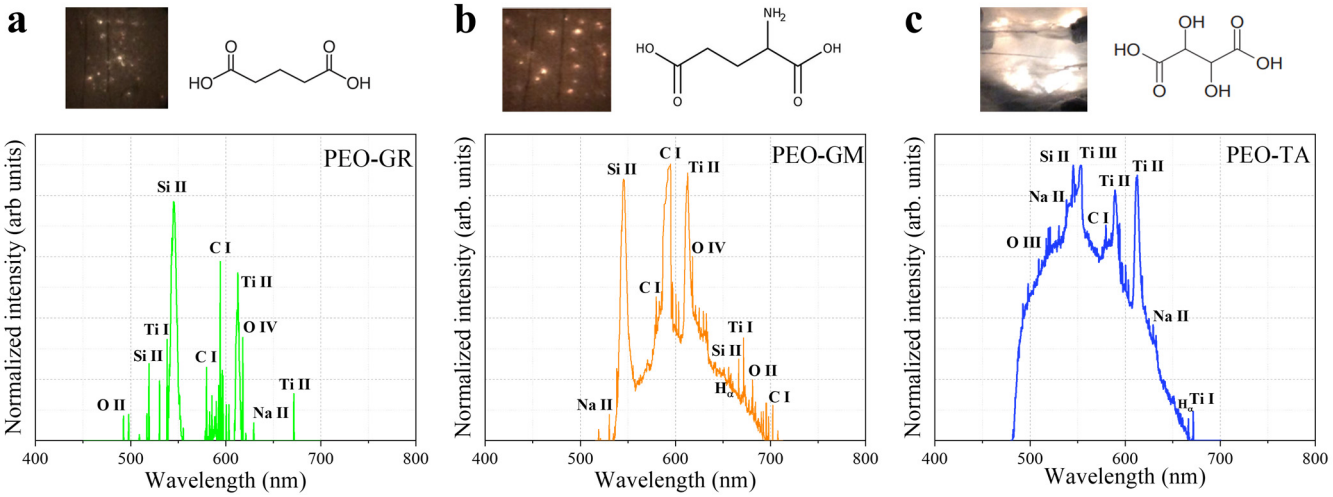

Figure 3. OES spectra of (**a**) PEO-GR, (**b**) PEO-GM, and (**c**) PEO-TA.

The spectrum of PEO-GR is less developed than the others, while PEO-TA shows a particularly intense background and signals related also to Ti III and O III species. Pictures acquired during the process agree with the intensity of the optical emission signal.

3.3. Structure and Morphology

3.3.1. X-ray Diffraction

The bulk structure of the oxide is investigated by XRD diffractograms performed in Bragg-Brentano geometry (Figure 4).

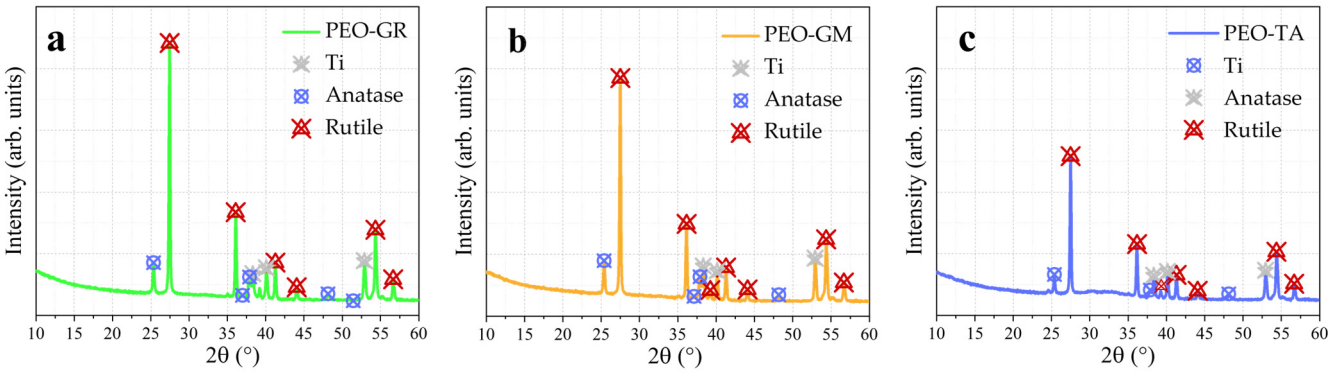

Figure 4. XRD diffractograms of (**a**) PEO-GR, (**b**) PEO-GM, and (**c**) PEO-TA.

Both anatase and rutile are present in all the coatings. Rutile is always the most abundant phase, and the most intense signals are collected for PEO-GR. The reflections

intensity, instead, is lower for PEO-TA, for which in the region between 30 and 35° it is possible to note a broad feature attributable to the contribution of amorphous silica [17].

An estimation of the contents of the two TiO_2 polymorphs (Table 2) is provided by using a modified Spurr–Meyer Equation (1).

$$X_R = \frac{1}{1 + 0.8\left(\frac{I_A}{I_R}\right)} \quad (1)$$

Table 2. Modified Spurr–Meyer XRD quantification results.

Sample	Anatase%	Rutile%
PEO-GR	8.84	91.16
PEO-GM	10.91	89.09
PEO-TA	13.4	86.60

I_A and I_R being the intensities of the highest XRD-peaks associated with anatase and rutile, found at 25.30° (Anatase—card number: PDF 00-064-0863) and 27.44° (Rutile—card number: PDF 01-089-0553), respectively. The modified Spurr–Meyer method assumes that the oxide layer is completely crystalline, so an overestimation of the real relative quantities is obtained. The validity of this assumption is questionable in the case of PEO-TA, because of the abundant presence of amorphous material. Nonetheless, the analysis can be used to express relative quantities with affordability. This evidence agrees with the lower intensity of all the reflections found in PEO-TA.

The addition of organic additives significantly modifies the structure of the PEO coatings with respect to that of an oxide produced using the same PEO parameters but without organic acids. In the latter case, rutile is the only crystalline structure of titanium oxide to be found (Supplementary Materials Figure S1), while when acids are added even anatase is produced. Moreover, the level of amorphism is strongly reduced when the organic additives are used.

3.3.2. SEM and EDS Analyses

SEM images of the samples' surface (Figure 5) highlight the presence of some common features for all the oxides as small pores, cracks, and acicular formations.

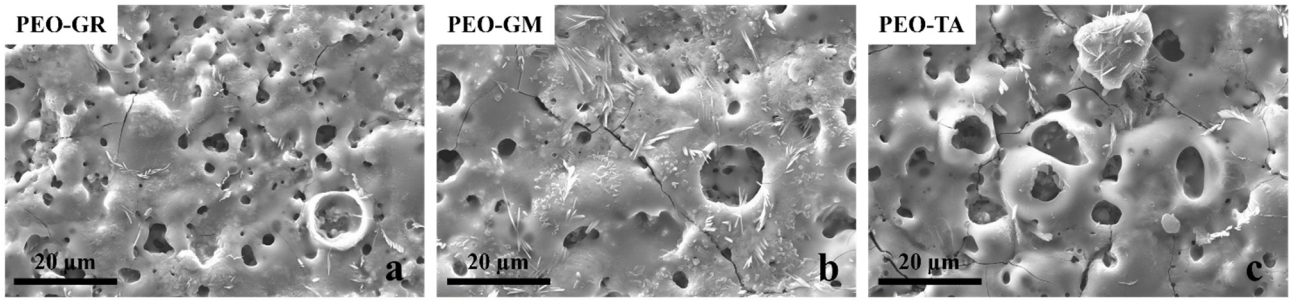

Figure 5. SEM images of the oxide surface of (**a**) PEO-GR, (**b**) PEO-GM, and (**c**) PEO-TA.

Working with glutaric acid, an oxide with a quite dense distribution of small pores (~3.28 ± 1.02 µm) and short cracks is obtained.

The surface of PEO-GM is crossed by long cracks which connect pores. The pore dimension varies from ~2.16 ± 0.59 µm for small, rounded holes, to about 7.95 ± 2.92 µm for crater-like structures. The presence of acicular morphology is particularly evident.

PEO-TA is characterized by the presence of globular structures, some of which are crossed by crater-like pores (~6.38 ± 1.66 µm), while in other cases small pores are formed at the boundary of these features. There are also some globules partially covered by acicular formations.

The globular formations noted for PEO-TA are observed even when the treatment is carried out working only with the base solution, without any organic acids (electrolytic bath consisting of NaOH 1 M + 0.03 M Na_2SiO_3, keeping constant all the other parameters). In this case, the globules are much more numerous and prominent, showing an almost spherical shape [18].

By looking at the EDS maps of the surfaces (Supplementary Materials Figure S2) it is possible to note that the concentration of Na is particularly high in correspondence with such acicular formations, while Ti seems to accumulate inside and around pores, probably as a consequence of the ejection of material caused by type-B discharges [19].

The EDS analyses also confirm what was noticed by in situ OES about the presence of elements belonging to both the electrolyte and the substrate in the oxide coating.

SEM (Figure 6) analyses are performed also on the cross-section of the PEO samples.

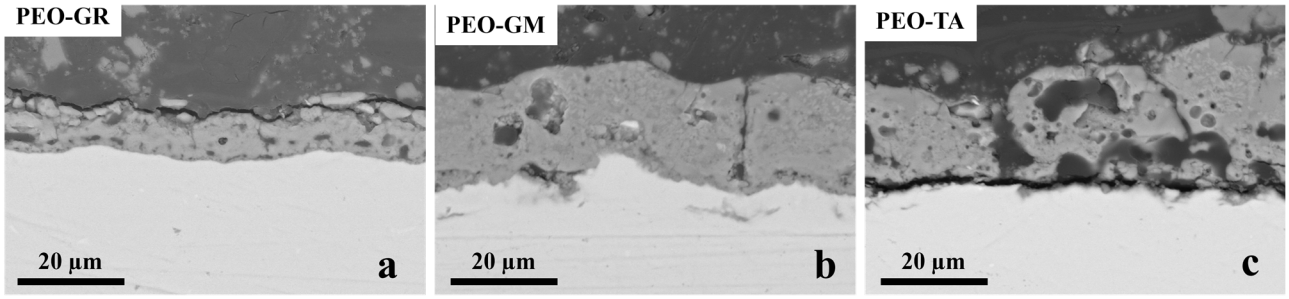

Figure 6. SEM images of the oxide cross-section of (**a**) PEO-GR, (**b**) PEO-GM, and (**c**) PEO-TA.

The coating of PEO-GR is quite thin, ~13 µm, but shows only small pores.

PEO-GM oxide is very thick, about 30 µm, and compact with only some large pores that are not interconnected with each other.

Using tartaric acid, a thick but highly defective layer is formed. There are large pores, which at the bottom of the coating are interconnected, and channels that cross the entire thickness of the oxide. A large and continuous crack cut the PEO-TA layer from the substrate, a sign that the adhesion of the coating is quite low.

The structures of the three coatings appear quite different from that of the oxide layer produced when PEO is performed in absence of organic additives. In the latter case, the coating is highly ununiform with sudden thickness variations (from 100 to 20 µm) due to the presence of defects and the detachment of portions of the coating because of lack of sintering of the oxide [18].

The EDS maps (Supplementary Materials Figure S3) of the cross-sections highlight that Si is mainly concentrated at the oxide/substrate interface, while Na content is larger in the external portion of the coatings.

3.3.3. GD-OES Analyses

For GD-OES analyses (Figure 7) relative intensities of the element signals, through the oxide thickness, are considered and each signal is multiplied for a constant factor for sake of representation.

Once again, the presence of elements coming from the electrolytic solutions is confirmed.

All the samples are characterized by a uniform distribution of O across the coating thickness, Na intensity is higher at the surface of the oxide while Si content slightly increases at the oxide/metal interface. Na and C intensities are particularly enhanced in the case of PEO-TA.

The C concentration significantly increases at the oxide/substrate interface and at the coating surface. Comparing the three spectra it is also possible to note that the C intensity at the oxide/substrate interface for samples prepared using glutamic acid is significantly lower than that of PEO-GR and PEO-TA.

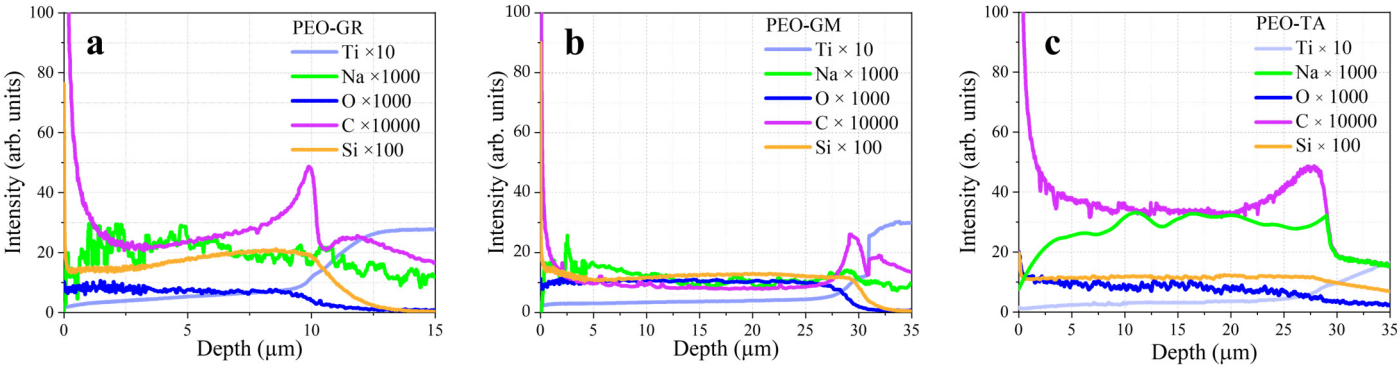

Figure 7. GD-OES spectra of (**a**) PEO-GR, (**b**) PEO-GM, and (**c**) PEO-TA.

Through GD-OES analysis it is also possible to obtain an estimation of the thickness of oxide coatings which results to be ~12 μm for PEO-GR, and ~30 μm for PEO-GM and PEO-TA, respectively.

3.4. Corrosion and Electrochemical Behaviour

3.4.1. Potentiodynamic Polarization Test

Figure 8 reports the potentiodynamic curves performed in a 10% *v*/*v* sulphuric acid solution at 60 °C. By means of the Tafel extrapolation, corrosion current density (i_{corr}), corrosion potential (E_{corr}) and cathodic Tafel coefficient (b_c) are derived (Table 3). Additionally, the polarization resistance, R_p, is calculated by using the Stern–Geray equation [5].

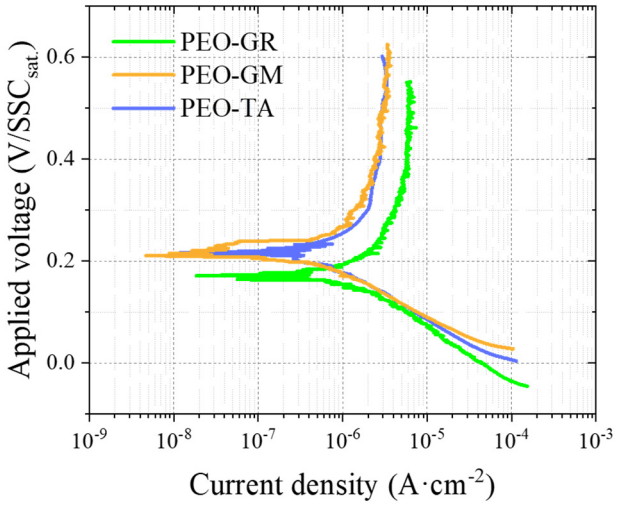

Figure 8. Tafel curves for PEO-GR, PEO-GM, and PEO-TA immersed in 10% *v*/*v* sulphuric acid at 60 °C.

Table 3. Data from Tafel extrapolation.

Sample	E_{corr} (mV/SSC$_{sat.}$)	b_c (mV·decade^{-1})	Rp (Ω·cm^2)	i_{corr} (mA·m^{-2})	CR (μm·y^{-1})
PEO-GR	169	121	1.4×10^5	1.68	2.94
PEO-GM	208	95	4.3×10^5	0.58	1.02
PEO-TA	197	99	2.4×10^5	1.05	1.84

All the samples display a free corrosion potential nobler than the bare metal (−668 mV/SSC$_{sat.}$) and a corrosion current density four orders of magnitude lower, proving the protection effect of the PEO coatings [18].

PEO-GM is characterized by the lowest corrosion current density which is one order of magnitude lower than those of the other samples.

According to b_c values, the cathodic reaction is hydrogen evolution with the Volmer step being the rate-determining step (120 mV of voltage increase for decade of current) [20].

3.4.2. Electrochemical Impedance Spectroscopy Test

Data obtained from EIS tests are plotted in Nyquist and Bode diagrams for all the samples (Figure 9).

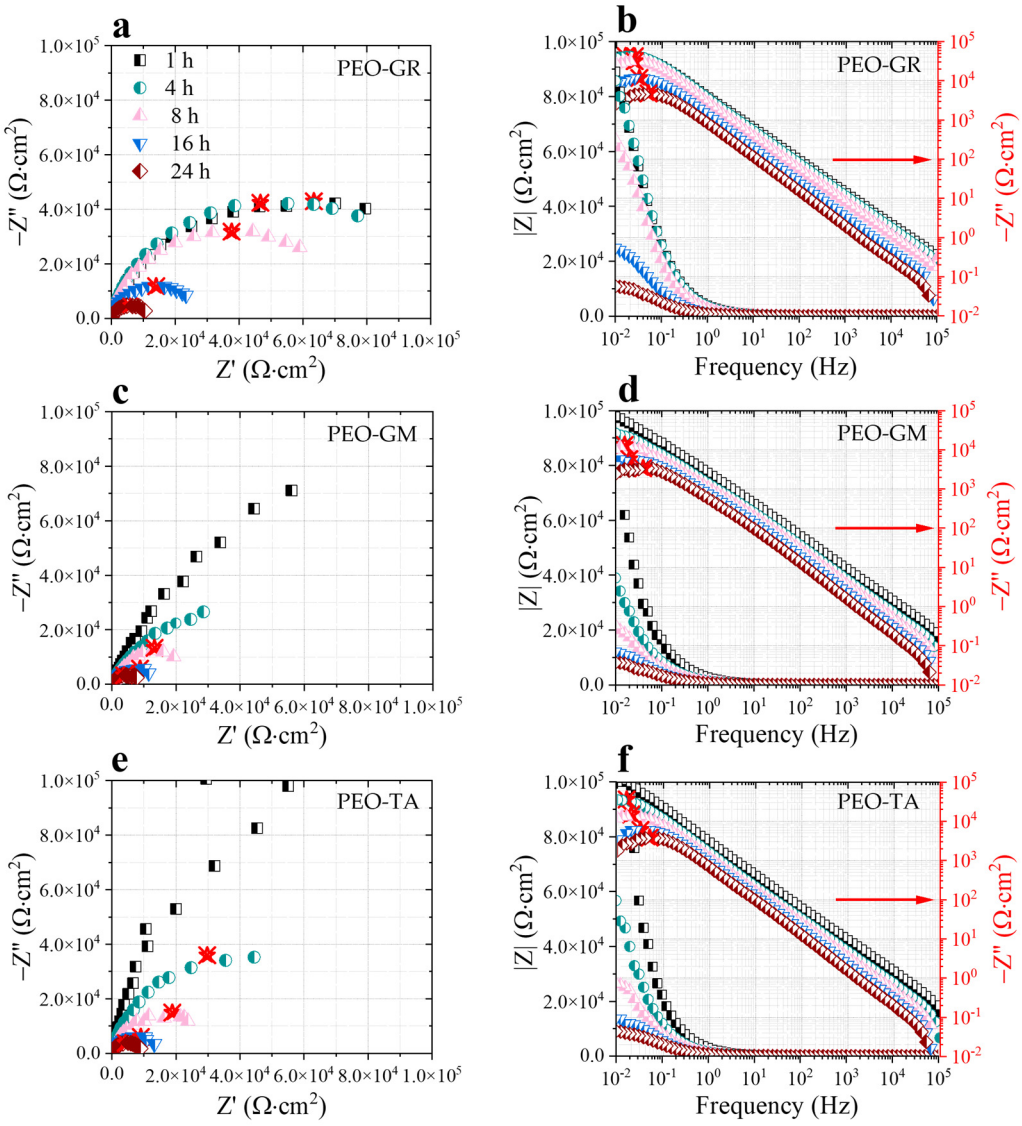

Figure 9. Nyquist and Bode representations of (**a**,**b**) PEO-GR, (**c**,**d**) PEO-GM, and (**e**,**f**) PEO-TA oxides immersed in 10% v/v sulphuric acid at 60 °C.

It is immediately noticeable that the Nyquist curves obtained for the PEO samples are significantly different from those of the untreated Ti Gr. 2. The coated specimens produce a single capacitive semicircle, while the bare material is characterized by a double capacitive loop which generally is observed when corrosion accompanied by hydrogen evolution takes place [18].

From the Nyquist curves it is possible to extrapolate the polarization resistance of the coating, R_p, defined as the intersection of the semicircles at $\omega \rightarrow 0$ with the Z′ axis, values are listed in Table 4 for all the samples with also the time constants extracted from the negative imaginary part of the impedance (indicated by the red stars in Figure 9).

Table 4. Polarization resistances, R_p, in $\Omega \cdot cm^2$ and time constant τ in s, derived from the Nyquist curves.

Sample	PEO-GR		PEO-GM		PEO-TA	
	R_p ($\Omega \cdot cm^2$)	τ (s)	R_p ($\Omega \cdot cm^2$)	τ (s)	R_p ($\Omega \cdot cm^2$)	τ (s)
1 h	1.17×10^5	64	2.03×10^5	/	9.12×10^5	/
4 h	1.17×10^5	40	5.75×10^4	/	1.01×10^5	63
8 h	8.40×10^4	40	2.80×10^4	63	3.58×10^4	50
16 h	2.91×10^4	25	1.29×10^4	50	1.49×10^4	31
24 h	1.16×10^4	20	8.24×10^3	25	9.30×10^3	16

The R_p values found after the first hour of immersion are in accordance with the results of potentiodynamic tests. All the values are in the order of magnitude 10^5 $\Omega \cdot cm^2$, however in the case of PEO-TA a slightly higher R_p is measured at the beginning of the EIS test.

The negative imaginary impedance is considered, given that this parameter was unaffected by the ohmic drop of the solution, thus providing direct insight into the time scale governing the corrosion reaction. In particular, PEO-GR presents a maximum even after 1 h of immersion. As the frequency of the occurrence of such a phenomenon is generally below 10^{-1} Hz it is reasonable to speculate the nature of a diffusion-related process inside the electrode, like proton transport. Being the time constant, describing diffusion processes, inversely proportional to the diffusion length, it is not strange to account for a peak in the negative imaginary part of Z even after 1 h of immersion of sample PEO-GR, whose thickness is about one third that of the other samples. On the other hand, the thickness and compactness found in PEO-GM do not allow the frequency window of the first two acquisitions to collect the relaxation of the diffusion process. However, the high level of crystallinity causes the electronic conduction to be considerably higher than the one observed for example in PEO-TA, resulting in lower R_p values, even if the proton transport along the oxide was considerably slower. This is not strange as the ionic conduction in a crystalline phase is more impervious, particularly in the rutile phase, whose crystal cell volume is considerably smaller than the one of the other TiO_2 polymorphs, for which values around 10^{-12} $cm^2 \cdot s^{-1}$ [21,22] are generally observed. Furthermore, the EIS tests reveal that all three types of PEO coatings, despite a copious decrease of R_p, keep the metallic substrate protected from the aggressive environment. This is demonstrated by the single semicircle present even after 24 h of immersion. It is well known that Ti, once activated, presents two well-resolved time constants [16,23].

4. Discussion

The experimental analyses carried out highlight a correlation between the functional groups of the organic additives and the final properties of the PEO coatings.

Depending on the functional groups, the interaction among the additives and the substrate changes influences the final structure and morphology of the oxide layers. The modification of such features strongly impacts the protective effect of the coatings against corrosive species, as highlighted by the results of the electrochemical tests.

4.1. Characterization of the PEO Process

The contribution of organic additives introduced into the electrolyte to plasma events is verified through OES analysis: indeed, signals related to C belonging to the acids are present in all the spectra, meaning that they participate in discharge processes.

The same is valid for the other additive of the electrolytic solution, Na_2SiO_3, whose involvement in plasma formation is confirmed by the intense Si II signals.

PEO with glutaric acid (PEO-GR) shows a less developed spectrum than the other samples. This is probably due to the occurrence of weaker discharges during anodization because of the formation of an adsorbed layer of glutarate ions on the metal surface

which partially shields it from the applied electric field and the electrolyte, preventing the development of highly energetic discharges.

Indeed, when describing the interaction between the treated Ti samples, the growing oxide, and the electrolytic species it is important to consider the possibility of anions adsorption onto the electrode surface, which may modify the charge transfer reaction immediately preceding the discharge event. The efficiency of the coverage of the surface provided by the anions strongly depends on the steric hindrance, the structure, the molecular weight, and the functional groups of the molecules that are involved in the PEO process [24,25].

In the present study, the influence of functional groups is found to be dominant while the effect of molecular weight is almost negligible in a first approximation since it is quite similar for the three acids (MW = 132.12, 147.13, 150.09 $g \cdot mol^{-1}$ for $C_5H_8O_4$, $C_5H_9NO_4$, and $C_4H_6O_6$ respectively).

4.2. Effect of the Functional Groups

Glutaric acid has two carboxyl groups that favour the interaction with the surface of the substrate by electron donation. The molecule is linear with only five C atoms along the backbone, permitting the formation of an ordered adsorbed layer. In this way, the interaction of both the carboxyl groups with the metal surface is permitted. Consequently, the alkyl chain of the molecules, with a weak electron-repelling character remained exposed to the solution, partially hindering the interaction with the electrolyte and preventing the growth of a thick oxide. As a result, an effective coverage of the anodic surface could be obtained, shielding it by the applied external electric field preventing too many destructive discharges from occurring.

In the case of *glutamic acid*, the interaction with the metal substrate should involve both the carboxyl groups according to what is explained in the introduction about the activation of the two groups depending on the applied potential. The steric hindrance is larger with respect to that of glutaric acid because of the presence of the lateral deprotonated amine group, and this can affect the efficiency of the coverage of the sample surface [26]. As a result, larger discharges with respect to the case of PEO-GR are produced, but typically they do not show a pronounced destructive character.

Tartaric acid has lateral –OH groups, which in the alkaline solution could be deprotonated [27–29]. Such groups not only increase the steric hindrance of tartaric acid molecules but when tartrates interact with the Ti surface through the carboxyl groups, the deprotonated $–O^-$ probably occupy lateral positions causing repulsions between adjacent molecules, preventing the formation of a uniform adsorbed layer able to protect the surface during plasma phenomena. Therefore, intense and static discharges are produced.

This phenomenon agrees with the highly intense signals recorded for PEO with tartaric acid in the OES spectrum. Among them, there are high O III-related lines, which are associated with the huge quantity of gas observed during the running of the treatment and probably in part also caused by the thermal decomposition of the organic matter. Thermal decomposition of tartaric acid, in particular, starts at about 169.85 °C and leads to the generation of water and carbon dioxide [30]. Such temperatures are easily achieved at the discharge sites that, when working with tartaric acid, are particularly numerous. Another peculiarity of PEO with the tartaric acid spectrum is the presence of Ti III signal, which is absent in all the other spectra and is indicative of the evaporation of titanium oxide through TiO molecules [21,31]. Moreover, it is important to note that C related lines when dealing with PEO-TA are considerably less intense than the ones observed with the other conditions, corroborating a lower participation of the organic anion to the spark events.

The occurrence of the interaction described above and so different for the three acids is more deeply investigated. Given also the different relaxation kinetics observed in the three electrolytes, EIS is performed at the free corrosion potential, E_{corr}, for Ti samples immersed in the PEO solutions (Nyquist diagrams are displayed in Figure 10, while the phase diagrams are reported in Supplementary Materials Figure S4). The result is fitted according to a simple Randle circuit where R_s and R_p are the solution and polarization

resistance and CPE is the constant phase element accounting for the distribution of time constants. An effective capacitance is extracted according to Brug's Equation (2) accounting for a surface distribution of time constant.

$$C_{eff.} = Y_0^{\frac{1}{n}} \left(\frac{1}{R_s} + \frac{1}{R_p} \right)^{\frac{n-1}{1}} \quad (2)$$

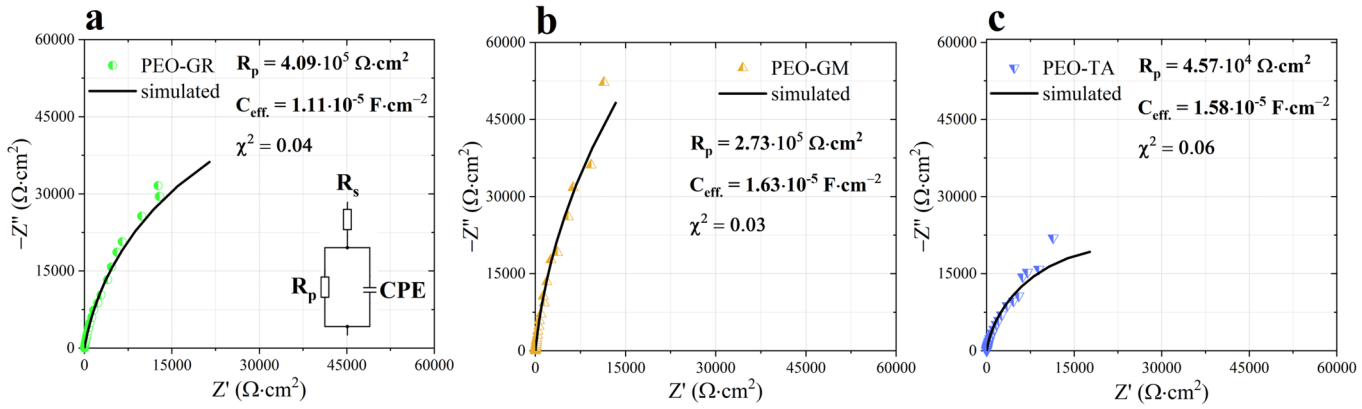

Figure 10. Nyquist diagrams of Ti samples immersed in the electrolytic solution used for producing (**a**) PEO-GR, (**b**) PEO-GM, and (**c**) PEO-TA.

All values extracted from circuit fitting are summarized in Table 5.

Table 5. Parameters extrapolated from the fitting of EIS data with a Randle circuit and C_{eff}. Calculated using the Brug's equation.

Sample	R_s ($\Omega \cdot cm^2$)	R_p ($\Omega \cdot cm^2$)	Y_0 ($s^n\ \Omega^{-1} \cdot cm^{-2}$)	n	$C_{eff.}$ ($F \cdot cm^{-2}$)	χ^2
PEO-GR	1.01	4.09×10^5	3.15×10^{-5}	0.91	1.11×10^{-5}	0.04
PEO-GM	1.08	2.73×10^5	2.99×10^{-5}	0.94	1.63×10^{-5}	0.03
PEO-TA	0.80	4.57×10^4	4.34×10^{-5}	0.91	1.58×10^{-5}	0.06

The higher R_p found for PEO with glutaric acid correlates with the stronger adsorption of glutarate anions, over the electrode surface, this attributed by its two carboxyl groups. This can prevent the adsorption of other species present in the PEO solution like hydroxide group, resulting in a lower C_{eff}. Very different figures are observed when dealing with PEO with tartaric acid. The different molecular arrangement, comprising two additional hydroxyl groups and one less C atom along its backbone, exerts profound differences in terms of the adsorption capability of the molecule. As a result, R_p diminished by one order of magnitude to $4.57 \times 10^4\ \Omega \cdot cm^2$ with respect to PEO-GR.

The results obtained for PEO-GM solution are in between those of the two previous electrolytes. This can be observed by R_p, with a value of $2.73 \times 10^5\ \Omega \cdot cm^2$ as the result of the action of the amine group present in glutamic acid. The interaction involving the amino acid generally occurs by bidentate chelating adsorption on the titanium surface promoted by the fact that glutamate at the present pH value can be considered completely deprotonated, thus a double negative charge, located near the two carboxyl groups can favour the adsorption [12,26].

4.3. Oxide Structure

Regarding the XRD diffractograms, as noted before, they reveal that TiO_2 is present as both anatase and rutile in all the samples. The base mechanism of titanium dioxide formation is described by reaction (3)

$$Ti^{4+} + 4OH^- \rightarrow TiO_2 + 2H_2O \quad (3)$$

where Ti^{4+} are the thermally activated cations coming from the metallic substrate, while the anions come from the electrolytic solution [5].

Interestingly, the lower rutile percentage is found for PEO-TA which shows a contribution coming from amorphous material, probably amorphous titanium oxide and primarily silica [32]. This condition can be explained according to the fact that the highly intense plasma events that are observed during the PEO process in presence of tartaric acid cause the formation of a large amount of molten material, which quickly solidifies because of the contact with the cold electrolyte. The rapid cooling does not allow the formation of a large amount of rutile (which is time-dependent) but leads to the generation of amorphous material. The presence of a high content of SiO_2 is related to the mechanism of retention of SiO_3^{2-} ions in the coating. The anions enter the oxide through the discharge channels due to the action of the intense electric field. Since the treatment of PEO-TA is characterized by numerous sparks, it is reasonable to assume that a certain quantity of SiO_3^{2-} is withdrawn within the discharge channels and then converted into amorphous SiO_2 according to reactions (4) and (5) [33,34]:

$$SiO_3^{2-} + 2H^+ \rightarrow SiO_2 + H_2O \quad (4)$$

$$SiO_3^{2-} \rightarrow 2SiO_2 + O_2 + 4e^- \quad (5)$$

The same mechanism of silica formation may occur even when the PEO treatment is carried out in the base solution without acids leading to the high level of amorphism highlighted in the diffractogram of the oxide (Figure S1). The amorphous structure of the PEO coating is also attributable to the generation of very intense plasma events causing the achievement of elevated temperatures in the molten material. Then the quenching occurring due to the contact with the electrolytic solution is so rapid that crystallization is limited, favouring the formation of an amorphous oxide.

4.4. Oxide Morphology

Observing the SEM images, it is possible to suppose a relationship between the occurrence of large and highly energetic discharges during PEO and the formation of large pores in the final oxide. Indeed, the smallest defects are observed on the surface of PEO-GR, which is associated with weak plasma events, while the largest pores and craters are those of PEO-TA, for which big static discharges are observed. When no organic acids are present the plasma can be even more aggressive than for PEO-TA since there is not any shielding effect provided by the adsorbed layer of organic molecules, thus a highly defective and inhomogeneous coating is produced.

Some pores of the PEO coatings are connected by cracks which probably originate because of the generation of thermal stresses during the cooling of the molten oxide and found a preferential propagation path across pores.

Pores and cracks could potentially be detrimental to the protective effect of the oxide from corrosion since the aggressive solution can penetrate through the defects easily reaching the inner layer of the oxide and the metal substrate.

The oxide morphology of PEO-TA differentiates from the others in the presence of globular structures over the surface. The formation of such globules may be due to the generation of high-pressure gas bubbles within the oxide. When such bubbles are surrounded by molten material, they could push the melted outward, causing the formation of globular features with central large pores. The longer the lifetime of the discharge, the longer the duration of the molten zone, and then larger spheres are produced at the surface. The central large pores are difficult to fill with melted material coming from new plasma events because of the presence of the globules themselves [18,35]. So, the final oxide will be crossed by large pores. This mechanism is more probable in the case of a melted oxide with high viscosity, as is the case for SiO_2 more than TiO_2, and according to the XRD spectrum, this hypothesis is more consistent in the cases of PEO-TA and the PEO oxide produced in absence of organic additives.

4.5. Oxide Composition

The EDS maps of the surface of the three samples show higher Na concentration in correspondence with the acicular formations. Therefore, it is possible to speculate the generation of sodium titanate. Titanates are generally characterized by acicular structure and can be generated by alkaline hydrothermal mechanism at relatively low temperature when crystalline TiO_2 is immersed in an aqueous NaOH solution [36]. The temperature increase that occurs during plasma events can be sufficient to promote the generation of such compound, which, indeed, are more concentrated in correspondence of pores or globules (in case of PEO-TA) where the higher temperatures are achieved.

By analysing the EDS images of the cross-section, it is noted that Si accumulates in the internal layers of the oxide. A possible explanation for this distribution relies again on the fact that field-driven SiO_3^{2-} anions enter the coating through the discharge channels and are withdrawn to the bottom of the oxide film. On the contrary, Na concentration is larger at the surface of the coating, a sign that this element is involved mainly in type-A and C plasma discharges which occur at the surface of the growing film [19].

The distribution of Si and Na is confirmed also by GD-OES spectra, which also highlights a specific trend for C profile. The C concentration significantly increases at the oxide/substrate interface and at the coating surface probably because of the adsorption and interaction of the organic molecules and anions on the metallic and oxide surfaces. Carbon signal is particularly high in case of PEO-TA, this may be due to the presence of several huge pores on whose surface tartrates could interact. On the other hand, the different C intensity observed between PEO-GR and PEO-GM can be the result of a different physical-chemical interaction of the two compounds with the substrate, stronger when dealing with glutarates, leading to higher C intensity inside the coating.

4.6. Corrosion and Electrochemical Behaviour

The potentiodynamic and EIS analyses highlight the primary role played by the coating's thickness.

PEO coatings produced with glutaric acid show the highest corrosion current density even if they are characterized by the most compact structure. This behaviour is associated with the reduced thickness which is almost one-third that of the oxide layers obtained using the other two organic acids. The small thickness allows a faster diffusion of aggressive ions through the oxide layer leading to the highest time constant during the first hours of immersion. However, the presence of only small defects in the glutaric acid treated coatings allows for minimizing the contact between the corrosive medium and the oxide layer, partially compensating for the disadvantage associated with the small thickness. This is clear looking at the evolution over time of the polarization resistance of the samples treated with glutaric acid which starting from about 4 h of the EIS test remains higher than that of PEO-coatings formed with tartaric acid for the entire duration of the analysis revealing a reliable anti-corrosion behaviour.

PEO-coatings produced with glutamic acid, instead, are characterized by the lowest corrosion current density (0.58 $mA \cdot m^{-2}$) and the lowest time constants for the diffusion process. Such a trend is due to the compactness of the oxide layer and its thickness. Indeed, the higher the thickness, the longer the time required for the diffusing of aggressive species, like protons, to reach the metallic substrate. Thus, for long exposure time, PEO samples treated with glutamic acid are highly advantaged with respect to those produced with the glutaric one and they efficiently limit the charge circulation from the electrolyte to the substrate providing great corrosion protection.

Finally, oxide coatings produced with tartaric acid show an intermediate corrosion current density. Even if the thickness of the oxide is comparable with that reached for treatment with glutamic acid, the coating obtained using tartaric acid is crossed by several long cracks and contains large pores and craters. All these defects are highly detrimental from the corrosion protection point of view since they facilitate the penetration of the aggressive electrolyte through the oxide layer and the contact between it and the Ti substrate

can easily occur. In addition, as highlighted by XRD analysis, coating produced using tartaric acid is characterized by the presence of amorphous phases which reduce the barrier effect towards ionic diffusion leading to a reduction of the time constant with respect to PEO with glutamic acid [37]. On the contrary, the prevalent crystalline structure of PEO with both glutaric and glutamic acids and the high content of rutile slower ions migration making more impervious H^+ diffusion through the bulk of the oxide. The contribution of rutile to the high corrosion resistance of oxide layers could also be associated with the low degree of lability characterizing Ti(IV) cations lowering the rate of exchange of oxygen ions to sulphate ions thus reducing the dissolution of the PEO coatings [38].

On the other hand, the lower level of crystallinity of coatings treated with tartaric acid reduces the electron transfer leading, in short exposure test, to the achievement of high R_p values. This justifies the quite unexpected result of EIS test with tartaric acid treated samples showing the highest polarization resistance for the first hour of immersion.

Another factor that influences the corrosion resistance of the oxides is the uniformity of the coating on the Ti surface. The more homogenous coating is obtained using glutamic acid, for which the treated samples are almost completely coated by the thick white oxide. The surface of the samples appears uniform even after the corrosion test, suggesting that the oxide dissolution occurs evenly. In the case of glutaric acid the oxide is less uniform as highlighted by the alternation of smaller white oxide regions and larger grey areas. Thus, corrosion occurs unevenly and at the end of the weight loss experiment, there are some small zones of the coupons where the oxide is completely removed. Oxide obtained in the presence of tartaric acid is the less uniform, especially at the edges of the specimens. Such regions exhibit a lower corrosion resistance than the central region of the samples, where the oxide layer is more even, and is principally involved in corrosion leading to the formation of wide exposed areas of the metal substrate after the immersion test, justifying the significant decrease of the polarization resistance.

5. Conclusions

The influence of organic acids on the properties of PEO coatings produced on titanium is found to mainly depend on the type and the number of functional groups present in the organic molecules. All three acids (glutaric, glutamic, and tartaric acid) are characterized by the presence of two carboxyl groups which probably are the main responsible for the interaction of the molecules with the metallic substrate and the growing oxide layer. Glutaric acid, which has only these two –COOH functional groups, strongly interacts with the titanium surface partially shielding it from the external electric field and the other electrolytic species, thus preventing the development of highly energetic plasma events. As a result, a thin but compact oxide layer is produced.

When an amine group is introduced, as it is for glutamic acid, the interaction of the organic molecules with the metallic substrate becomes weaker due to their larger steric hindrance related to the deprotonated amine groups. This weaker interaction leads to the occurrence of more energetic discharges that on one hand cause the formation of larger defects, but on the other hand, allow to produce thicker coatings.

The effect of the functional groups becomes even more evident working with tartaric acid that displays two hydroxyl groups in addition to the carboxyl ones. In this case, plasma is particularly intense and unevenly distributed large discharges are produced on the titanium specimens. The ceramic-like layer produced exhibits a less uniform and defective structure among the three types of coatings. The presence of huge pores and cracks significantly affects the protective behaviour of PEO coatings, then the samples treated with tartaric acid are characterized by the largest reduction of the polarization resistance over time.

On the contrary, PEO treatment performed using glutaric and especially glutamic acid allows to produce coatings with an enhanced anti-corrosive effect, as proved by the relatively low values of corrosion current density (~0.58 $mA \cdot m^{-2}$ for coatings produced with glutamic acid) and the high polarization resistance values (~1.2 $\times$ 10^4 $\Omega \cdot cm^2$ for

glutaric acid treated samples). This high corrosion resistance is the consequence of the compact structure and the high degree of crystallinity of the oxide layers, which the penetration of aggressive substances as well as the migration of protons. In particular, the best performance in terms of corrosion protection, is provided by coatings obtained through the PEO process performed in the presence of glutamic acid. Such coatings not only show the advantageous structure described above but are also thick (~30 µm), further slowing down the diffusion of aggressive species towards the metallic substrate showing an improved and reliable protective effect.

Supplementary Materials: The following supporting information can be downloaded at: https://www.mdpi.com/article/10.3390/coatings14060703/s1, Figure S1: XRD diffractogram of PEO oxide produced in absence of organic acids; Figure S2: EDS maps of the surface of PEO coatings where the color code is oxygen in turquoise, sodium in orange, silicon in red, and titanium in blue; Figure S3: EDS maps of the cross-section of PEO coatings where the color code is oxygen in yellow, sodium in green, silicon in pink, and titanium in blue; Figure S4: Phase diagrams of Ti samples immersed in the electrolytic solution used for producing PEO-GR, PEO-GM, and PEO-TA.

Author Contributions: F.C.: conceptualization, experimental design, data collection, editing, and writing. L.C.: conceptualization, experimental design, data collection, editing, and writing. M.O.: conceptualization, experimental design, data collection, editing, and writing. All authors have read and agreed to the published version of the manuscript.

Funding: This research received no external funding.

Institutional Review Board Statement: Not applicable.

Informed Consent Statement: Not applicable.

Data Availability Statement: The data presented in this study are available on request from the corresponding author.

Conflicts of Interest: The authors declare no conflicts of interest.

References

1. Sun, S.; Lv, W. Microstructure and Mechanical Properties of TC18 Titanium Alloy. *Xiyou Jinshu Cailiao Yu Gongcheng/Rare Met. Mater. Eng.* **2016**, *45*, 1138–1141. [CrossRef]
2. Prando, D.; Brenna, A.; Bolzoni, F.M.; Diamanti, M.V.; Pedeferri, M.; Ormellese, M. Electrochemical Anodizing Treatment to Enhance Localized Corrosion Resistance of Pure Titanium. *J. Appl. Biomater. Funct. Mater.* **2017**, *15*, e19–e24. [CrossRef] [PubMed]
3. Schwartz, A.; Kossenko, A.; Zinigrad, M.; Danchuk, V.; Sobolev, A. Cleaning Strategies of Synthesized Bioactive Coatings by PEO on Ti-6Al-4V Alloys of Organic Contaminations. *Materials* **2023**, *16*, 4624. [CrossRef]
4. Kurup, A.; Dhatrak, P.; Khasnis, N. Surface Modification Techniques of Titanium and Titanium Alloys for Biomedical Dental Applications: A Review. *Mater. Today Proc.* **2020**, *39*, 84–90. [CrossRef]
5. Shokouhfar, M.; Dehghanian, C.; Montazeri, M.; Baradaran, A. Preparation of Ceramic Coating on Ti Substrate by Plasma Electrolytic Oxidation in Different Electrolytes and Evaluation of Its Corrosion Resistance: Part II. *Appl. Surf. Sci.* **2012**, *258*, 2416–2423. [CrossRef]
6. Sikdar, S.; Menezes, P.V.; Maccione, R.; Jacob, T.; Menezes, P.L. Plasma Electrolytic Oxidation (Peo) Process—Processing, Properties, and Applications. *Nanomaterials* **2021**, *11*, 1375. [CrossRef]
7. Aliofkhazraei, M.; Macdonald, D.D.; Matykina, E.; Parfenov, E.V.; Egorkin, V.S.; Curran, J.A.; Troughton, S.C.; Sinebryukhov, S.L.; Gnedenkov, S.V.; Lampke, T.; et al. Review of Plasma Electrolytic Oxidation of Titanium Substrates: Mechanism, Properties, Applications and Limitations. *Appl. Surf. Sci. Adv.* **2021**, *5*, 100121. [CrossRef]
8. Nashrah, N.; Putri, R.A.K.; Alharissa, E.Z.; Al Zoubi, W.; Ko, Y.G. Hybrid Organic-Inorganic Materials on Metallic Surfaces: Fabrication and Electrochemical Performance. *Metals* **2021**, *11*, 1043. [CrossRef]
9. Lin, B.; Zuo, Y. Corrosion Inhibition of Carboxylate Inhibitors with Different Alkylene Chain Lengths on Carbon Steel in an Alkaline Solution. *RSC Adv.* **2019**, *9*, 7065–7077. [CrossRef]
10. Spah, M.; Spah, D.C.; Deshwal, B.; Lee, S.; Chae, Y.K.; Park, J.W. Thermodynamic Studies on Corrosion Inhibition of Aqueous Solutions of Amino/Carboxylic Acids toward Copper by EMF Measurement. *Corros. Sci.* **2009**, *51*, 1293–1298. [CrossRef]
11. Kornyushova, E.A.; Kashevskii, A.V.; Arsent'ev, K.Y.; Pushkarev, B.G.; Nikiforov, S.B.; Safronov, A.Y. Electrochemical Behavior of Titanium and Platinum in Dicarboxilic Amino Acids Solution. *Bioelectrochemistry* **2019**, *126*, 113–120. [CrossRef] [PubMed]
12. Šarac, B.; Hadži, S. Analysis of Protonation Equilibria of Amino Acids in Aqueous Solutions Using Microsoft Excel. *J. Chem. Educ.* **2021**, *98*, 1001–1007. [CrossRef]

13. Yu, M.; Liang, H.; Liu, J.; Wu, L.; Li, X.; Zhu, M. Effect of Tartaric Acid on Anodic Behaviour of Titanium Alloy. *Surf. Eng.* **2015**, *31*, 912–918. [CrossRef]
14. Friedemann, A.E.R.; Gesing, T.M.; Plagemann, P. Electrochemical Rutile and Anatase Formation on PEO Surfaces. *Surf. Coat. Technol.* **2017**, *315*, 139–149. [CrossRef]
15. Nominé, A.; Nominé, A.V.; Braithwaite, N.S.J.; Belmonte, T.; Henrion, G. High-Frequency-Induced Cathodic Breakdown during Plasma Electrolytic Oxidation. *Phys. Rev. Appl.* **2017**, *8*, 031001. [CrossRef]
16. Casanova, L.; La Padula, M.; Pedeferri, M.P.; Diamanti, M.V.; Ormellese, M. An Insight into the Evolution of Corrosion Resistant Coatings on Titanium during Bipolar Plasma Electrolytic Oxidation in Sulfuric Acid. *Electrochim. Acta* **2021**, *379*, 138190. [CrossRef]
17. Lu, X.; Shih, K.; Li, X.Y.; Liu, G.; Zeng, E.Y.; Wang, F. Accuracy and Application of Quantitative X-Ray Diffraction on the Precipitation of Struvite Product. *Water Res.* **2016**, *90*, 9–14. [CrossRef]
18. Ceriani, F.; Casanova, L.; Massimini, L.; Brenna, A.; Ormellese, M. TiO_2 Microparticles Incorporation in Coatings Produced by Plasma Electrolytic Oxidation (PEO) on Titanium. *Coatings* **2023**, *13*, 1718. [CrossRef]
19. Hussein, R.O.; Nie, X.; Northwood, D.O. A Spectroscopic and Microstructural Study of Oxide Coatings Produced on a Ti-6Al-4V Alloy by Plasma Electrolytic Oxidation. *Mater. Chem. Phys.* **2012**, *134*, 484–492. [CrossRef]
20. Murthy, A.P.; Theerthagiri, J.; Madhavan, J. Insights on Tafel Constant in the Analysis of Hydrogen Evolution Reaction. *J. Phys. Chem. C* **2018**, *122*, 23943–23949. [CrossRef]
21. Casanova, L.; Arosio, M.; Taghi Hashemi, M.; Pedeferri, M.P.; Botton, G.A.; Ormellese, M. A Nanoscale Investigation on the Influence of Anodization Parameters during Plasma Electrolytic Oxidation of Titanium by High-Resolution Electron Energy Loss Spectroscopy. *Appl. Surf. Sci.* **2021**, *570*, 151133. [CrossRef]
22. Hupfer, A.J.; Monakhov, E.V.; Svensson, B.G.; Chaplygin, I.; Lavrov, E.V. Hydrogen Motion in Rutile TiO_2. *Sci. Rep.* **2017**, *7*, 17065. [CrossRef] [PubMed]
23. Lasia, A. Applications of Electrochemical Impedance Spectroscopy to Hydrogen Adsorption. In *Modern Aspects of Electrochemistry*; Springer: Boston, MA, USA, 2002; pp. 1–49.
24. Casanova, L.; Ceriani, F.; Pedeferri, M.; Ormellese, M. Addition of Organic Acids during PEO of Titanium in Alkaline Solution. *Coatings* **2022**, *12*, 143. [CrossRef]
25. Kaseem, M.; Dikici, B. Optimization of Surface Properties of Plasma Electrolytic Oxidation Coating by Organic Additives: A Review. *Coatings* **2021**, *11*, 374. [CrossRef]
26. Ustunol, I.B.; Gonzalez-Pech, N.I.; Grassian, V.H. PH-Dependent Adsorption of α-Amino Acids, Lysine, Glutamic Acid, Serine and Glycine, on TiO2 Nanoparticle Surfaces. *J. Colloid Interface Sci.* **2019**, *554*, 362–375. [CrossRef] [PubMed]
27. Beck, M.; Csiszar, B.; Szarvas, P. Acidic Dissociation Constant of Alcoholic Hydroxyls of Hydroxycarboxylic Acids: Tartaric Acid. *Nat. Publ. Gr.* **1960**, *188*, 846–847. [CrossRef]
28. Motekaitis, R.; Martell, A. Aluminum(II1) with Hydroxy Carboxylic Acids. *Inorg. Chem.* **1984**, *23*, 18–23. [CrossRef]
29. Bezryadin, S.G.; Chevela, V.V.; Ajsuvakova, O.P.; Ivanova, V.Y.; Kuzyakin, D.V. Titanium(Iv) Tartrate Complexes in Aqueous Solutions. *Russ. Chem. Bull.* **2015**, *64*, 2655–2662. [CrossRef]
30. Fukami, T.; Tahara, S.; Yasuda, C.; Nakasone, K. Structural Refinements and Thermal Properties of L(+)-Tartaric, D(–)-Tartaric, and Monohydrate Racemic Tartaric Acid. *Int. J. Chem.* **2016**, *8*, 9. [CrossRef]
31. Kitamura, T.; Shibata, K.; Takeda, K. In-Flight Reduction of Fe_2O_3, Cr_2O_3, TiO_2 and Al_2O_3 by Ar-H_2 and Ar-CH4 Plasma. *ISIJ Int.* **1994**, *33*, 1150–1158. [CrossRef]
32. Čolović, B.; Kisić, D.; Jokanović, B.; Rakočević, Z.; Nasov, I.; Petkoska, A.T.; Jokanović, V. Wetting Properties of Titanium Oxides, Oxynitrides and Nitrides Obtained by DC and Pulsed Magnetron Sputtering and Cathodic Arc Evaporation. *Mater. Sci. Pol.* **2019**, *37*, 173–181. [CrossRef]
33. Dehnavi, V.; Luan, B.L.; Shoesmith, D.W.; Liu, X.Y.; Rohani, S. Effect of Duty Cycle and Applied Current Frequency on Plasma Electrolytic Oxidation (PEO) Coating Growth Behavior. *Surf. Coat. Technol.* **2013**, *226*, 100–107. [CrossRef]
34. Stojadinović, S.; Vasilić, R.; Petković, M.; Kasalica, B.; Belča, I.; Žekić, A.; Zeković, L. Characterization of the Plasma Electrolytic Oxidation of Titanium in Sodium Metasilicate. *Appl. Surf. Sci.* **2013**, *265*, 226–233. [CrossRef]
35. Zhang, X.; Aliasghari, S.; Němcová, A.; Burnett, T.L.; Kuběna, I.; Šmíd, M.; Thompson, G.E.; Skeldon, P.; Withers, P.J. X-Ray Computed Tomographic Investigation of the Porosity and Morphology of Plasma Electrolytic Oxidation Coatings. *ACS Appl. Mater. Interfaces* **2016**, *8*, 8801–8810. [CrossRef]
36. Liu, J.; Wang, B.; Banis, M.N.; Wang, Z.; Li, R.; Wang, J.; Hu, Y.; Sham, T.K.; Sun, X. Investigation of Amorphous to Crystalline Phase Transition of Sodium Titanate by X-Ray Absorption Spectroscopy and Scanning Transmission X-Ray Microscopy. *Can. J. Chem.* **2017**, *95*, 1163–1169. [CrossRef]

37. Minhas, B.; Dino, S.; Zuo, Y.; Qian, H.; Zhao, X. Improvement of Corrosion Resistance of TiO_2 Layers in Strong Acidic Solutions by Anodizing and Thermal Oxidation Treatment. *Materials* **2021**, *14*, 1188. [CrossRef]
38. Dubenko, A.V.; Nikolenko, M.V.; Aksenenko, E.V.; Kostyniuk, A.; Likozar, B. Mechanism, Thermodynamics and Kinetics of Rutile Leaching Process by Sulfuric Acid Reactions. *Processes* **2020**, *8*, 640. [CrossRef]